

Filter Images First, Generate Instructions Later: Pre-Instruction Data Selection for Visual Instruction Tuning

Bardia Safaei^{1*}, Faizan Siddiqui², Jiacong Xu¹, Vishal M. Patel¹, Shao-Yuan Lo²

¹Johns Hopkins University, ²Honda Research Institute USA

{bsafaei1, jxu155, vpatel36}@jhu.edu {faizan.siddiqui, shao-yuan_lo}@honda-ri.com

Abstract

Visual instruction tuning (VIT) for large vision-language models (LVLMs) requires training on expansive datasets of image-instruction pairs, which can be costly. Recent efforts in VIT data selection aim to select a small subset of high-quality image-instruction pairs, reducing VIT runtime while maintaining performance comparable to full-scale training. However, a major challenge often overlooked is that generating instructions from unlabeled images¹ for VIT is highly expensive. Most existing VIT datasets rely heavily on human annotations or paid services like the GPT API, which limits users with constrained resources from creating VIT datasets for custom applications. To address this, we introduce Pre-Instruction Data Selection (PreSel), a more practical data selection paradigm that directly selects the most beneficial unlabeled images and generates instructions only for the selected images. PreSel first estimates the relative importance of each vision task within VIT datasets to derive task-wise sampling budgets. It then clusters image features within each task, selecting the most representative images with the budget. This approach reduces computational overhead for both instruction generation during VIT data formation and LVLM fine-tuning. By generating instructions for only 15% of the images, PreSel achieves performance comparable to full-data VIT on the LLaVA-1.5 and Vision-Flan datasets. The link to our project page: <https://bardisafa.github.io/PreSel>

1. Introduction

Recent advances in large vision-language models (LVLMs) [2, 7, 21, 22, 50] have demonstrated remarkable capabilities in complex multimodal reasoning and human instruction following. Visual instruction tuning (VIT) is a crucial stage in training LVLMs, enabling these models

¹Throughout the paper, we refer to images without corresponding textual instructions as unlabeled images.

*This work was mostly done when B. Safaei was an intern at HRI-USA.

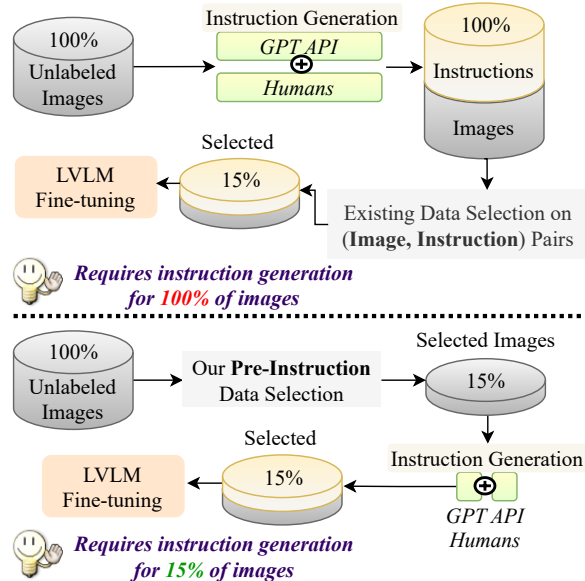


Figure 1. **Top:** Existing VIT data selection methods assume access to well-prepared VIT datasets in which all the images are already annotated with instructions by costly resources, such as GPT API and human labor. These methods require information on both images and their instructions. **Bottom:** Our approach performs selection directly on unlabeled images and then utilizes resources to generate instructions exclusively for the selected images. Hence, we not only enable faster fine-tuning but also significantly reduce instruction generation costs (e.g., 15%).

to follow instructions and generalize across various tasks. VIT datasets [22, 44, 46] contain visual instructions from a diverse range of vision tasks, such as visual question answering (VQA) [10, 27, 36], optical character recognition (OCR) [29], visual grounding [13], captioning [37], etc. A typical VIT sample is an image-instruction pair consisting of an unlabeled image and instructions generated by human labor or paid services such as the GPT API [1, 3, 32]. However, two key challenges arise with the current VIT process: (1) Combining visual instructions from diverse

tasks could lead to data redundancy, largely increasing training time while yielding only marginal performance gains. (2) Generating high-quality instructions is highly expensive. Specifically, synthesizing instructions from unlabeled images via services like GPT-4 [1] incurs significant API costs. Furthermore, human involvement is often required to ensure instruction quality, such as in image-grounded question generation, response consistency, and removal of factually incorrect questions.

Recently, several data selection methods for VIT [5, 15, 24, 40] have attempted to solve the data redundancy issue by selecting a small subset of informative image-instruction pairs and fine-tuning LVLMs on this subset only, thereby reducing training time. Still, the high-cost issue of instruction generation for large-scale VIT datasets remains overlooked. These methods assume access to well-prepared VIT datasets in which all the images are already annotated with instructions, and their data selection algorithms require information on both images and the corresponding instructions. Hence, these methods are less useful when users need to create new VIT datasets for their custom applications but have limited resources to generate high-quality instructions. To address this, we pose the following question: *“Given a large-scale collection of unlabeled images from multiple vision tasks, how can we select the most impactful images for LVLM fine-tuning before the costly instruction generation step?”* Answering this question would allow us to allocate resources to generate instructions only for the selected images.

In this paper, we propose a novel Pre-instruction data Selection approach, termed PreSel, a more practical data selection paradigm that not only reduces dataset size for faster fine-tuning but also significantly cuts down instruction generation costs (see Figure 1). PreSel consists of two stages: (1) task-importance estimation and (2) task-wise cluster-based selection. In a typical VIT dataset, the quantity of data is unbalanced across different vision tasks, and this quantity distribution can greatly impact LVLM performance [8, 15]. Unlike prior works that use heuristic methods to balance task data [33, 39, 43], our Stage 1 introduces an automated task-importance estimation process. It begins by randomly sampling a small fraction of unlabeled images from each task (e.g., as little as 5%) and obtaining instructions for them. Using this small reference set, we propose the *Instruction Relevance Score (IRS)* to compute the relative importance of each task. The importance values determine task-wise sampling budgets for data selection. Next, Stage 2 employs a lightweight vision encoder (e.g., DINOv2 [30]) to extract features for the unlabeled images in each task, and performs clustering to select the most representative images within each cluster. Finally, instructions are acquired for the selected images, preparing them for LVLM fine-tuning.

We verify the effectiveness of PreSel on two large-scale VIT datasets: LLaVA-1.5 [22] and Vision-Flan [44].

Our experiments assume that these datasets consist solely of unlabeled images to simulate the more practical pre-instruction selection scenario. Using only 15% of the VIT data, PreSel achieves performance comparable to LVLMs fine-tuned on the full dataset. Notably, this efficiency is attained by pre-instruction data selection, which requires only 15% of the instruction generation cost. We also demonstrate the transferability of PreSel’s selection to LVLMs across various architectures and sizes. We release our selected subset to the public to facilitate efficient model development. To the best of our knowledge, we are the first to introduce the pre-instruction VIT data selection paradigm, operating on unlabeled images before instruction generation. The key contributions are summarized as follows.

- We are the first to introduce the pre-instruction VIT data selection paradigm, a more practical data selection paradigm that reduces not only VIT runtime but also instruction generation cost.
- We propose PreSel, a novel pre-instruction data selection approach that operates on unlabeled images before instruction generation.
- Experiments on LLaVA-1.5 and Vision-Flan show that, using only 15% of the data and instruction generation cost, PreSel achieves performance comparable to LVLMs fine-tuned on the full VIT dataset.

2. Related Work

Visual Instruction Tuning. Instruction tuning is an essential training step that enables large language models (LLMs) to follow instructions and generalize across various tasks [1, 6, 9, 32]. Recent advances, such as LLaVA [21, 22], MiniGPT-4 [50], InstructBLIP [7] and Qwen-VL-Chat [2], extend this technology from the natural language processing (NLP) domain to multi-modality, i.e., VIT for fine-tuning LVLMs. These works include large-scale VIT data, which demands considerable LVLM training time. Moreover, to create such large-scale VIT datasets, these works mostly employ GPT-family models [1, 3, 32] to synthesize visual instructions from unlabeled images, with human involvement often needed to ensure instruction quality. This instruction generation process is highly expensive.

Data Selection for Visual Instruction Tuning. Due to high training costs, recent studies have investigated data-efficient instruction tuning [19, 41, 49]. LIMA [49] is the first to show that training LLMs on a selected small subset of data can reach same-level performance. LESS [41] designs an optimizer-aware algorithm to estimate data influences. Li et al. [19] develop the Instruction-Following Difficulty (IFD) metric to select essential data.

Several recent attempts further explore data selection for VIT [5, 15, 24, 40]. InstructionGPT-4 [40] uses metrics such as CLIP- and GPT-based scores to select high-quality

VIT samples, but its fine-tuning results are suboptimal. Self-Filter [5] first trains a score-net along with LVLM fine-tuning on all VIT data and then uses the score-net to select a data subset for a second round of VIT. However, this double-round process increases the overall training cost, contradicting the motivation of data selection. Liu et al. [24] leverage gradients to estimate the importance of each sample, yet the gradient information is expensive as it requires back-propagating the target LVLM. COINCIDE [15] introduces a clustering method to identify concept-skill compositions for LVLMs, but it needs instructions as references in its process.

While these VIT data selection methods achieve comparable performance using only a small portion of data, their selection pipelines require full access to image-instruction pairs. In contrast, our approach performs selection directly on unlabeled images, generating instructions only for the selected ones. Hence, we not only enable faster fine-tuning but also significantly reduce instruction generation costs.

3. Methodology

In this section, we first formulate the problem of pre-instruction data selection for visual instruction tuning and then elaborate on the proposed approach.

Problem Formulation. Consider a large pool of unlabeled images \mathcal{D} assembled from various datasets to construct a VIT dataset with M distinct vision tasks $\{T_i\}_{i=1}^M$, where $\mathcal{D} = \bigcup_{i=1}^M T_i$, and we denote the number of samples in \mathcal{D} as $|\mathcal{D}|$. Examples of vision tasks include VQA, OCR, etc., and each task T_i consists of a set of unlabeled images $T_i = \{I_a^i\}_{a=1}^{|T_i|}$. Note that tasks may overlap in images, i.e., $T_i \cap T_j \neq \emptyset$ for some $i \neq j$. For an unlabeled image I from task T_i , the corresponding textual instruction Y is generated as $Y = F_i(I)$, where F_i represents the instruction generation process for T_i . Note that F_i is not a straightforward mathematical function; rather, it is a costly, task-specific procedure, potentially involving resources such as the GPT API [1, 3] or human annotators who label images with instructions based on defined guidelines.

The goal of pre-instruction data selection is to select a small subset of highly beneficial unlabeled images $\mathcal{D}_S \subset \mathcal{D}$, where $|\mathcal{D}_S| \ll |\mathcal{D}|$, and then it only acquires instructions for this small subset. Fine-tuning an LVLM on the resulting image-instruction pairs, $\{(I_a, Y_a)\}_{a=1}^{|\mathcal{D}_S|}$, should maximally improve the LVLM’s instruction-following capabilities and achieve performance comparable to full-scale fine-tuning on \mathcal{D} with complete instructions: $\{(I_a, Y_a)\}_{a=1}^{|\mathcal{D}|}$. The key difference between the pre-instruction data selection paradigm and existing VIT data selection methods is that the latter assumes access to instructions of all images (i.e., $\{(I_a, Y_a)\}_{a=1}^{|\mathcal{D}|}$), while pre-instruction data selection solely relies on unlabeled images $\{I_a\}_{a=1}^{|\mathcal{D}|}$ for selecting \mathcal{D}_S . Hence, this paradigm enables efficiency in both training and instruction generation.

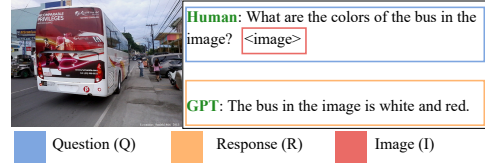


Figure 2. An illustration of Q , R , and I in a VIT sample. Instruction $Y = \{Q, R\}$.

Overview. Our approach begins with a Task-Importance Estimation mechanism to obtain the optimal proportion of each task T_i in \mathcal{D}_S . To achieve this, we first randomly select a small reference set of images $\mathcal{D}_{\text{ref}} \subset \mathcal{D}$, where $|\mathcal{D}_{\text{ref}}| \ll |\mathcal{D}_S| \ll |\mathcal{D}|$, and acquire their corresponding instructions, $\{(I_a, Y_a)\}_{a=1}^{|\mathcal{D}_{\text{ref}}|}$. Each instruction Y_a is then decomposed into questions Q_a and responses R_a (i.e., $Y_a = \{Q_a, R_a\}$; see Figure 2), which are used to compute our proposed *Instruction Relevance Score (IRS)* for the samples in \mathcal{D}_{ref} . The average IRS over images in each task T_i determines the relative proportions of these tasks in \mathcal{D}_S , termed $w(T_i)$. Next, we employ a lightweight vision encoder, e.g., DINOv2 [30], to extract visual features for the remaining unlabeled images and cluster them in each task. Finally, given the derived task proportion $w(T_i)$, the most representative images from each cluster are selected via the *Neighbor Centrality (NC)* score.

3.1. Task-Importance Estimation

Determining an appropriate proportion of samples from each task for the final selected subset \mathcal{D}_S is crucial. Simply relying on the number of images available per task to set these proportions can lead to suboptimal performance, as tasks often differ in their levels of redundancy. Also, some tasks may be effectively learned through training on related tasks, making direct sampling from them less essential [8, 15].

We start by fine-tuning the target LVLM on the image-instruction pairs in a randomly selected small reference set \mathcal{D}_{ref} , which comprises only a small fraction (e.g., as little as 5%) of the entire VIT dataset \mathcal{D} . This initial fine-tuning, conducted for one epoch, equips the LVLM with basic instruction-following abilities. We refer to this fine-tuned model as the *reference model*. Inspired by the loss-based data selection methods in NLP [19, 28], we extend the loss-based idea to address the more complicated multimodal scenario and leverage the loss predictions of the reference model on \mathcal{D}_{ref} to define our *Instruction Relevance Score (IRS)* for estimating task importance.

As shown in Figure 2, each VIT example in \mathcal{D}_{ref} is represented as a triplet (I, Q, R) , where I represents the image, Q the textual question (from a human), and R the response (from GPT). Q and R may extend over multiple interaction rounds. The proposed IRS is calculated by comparing the reference model’s next-token cross-entropy (CE) loss with and without the Q tokens as part of the input. This score

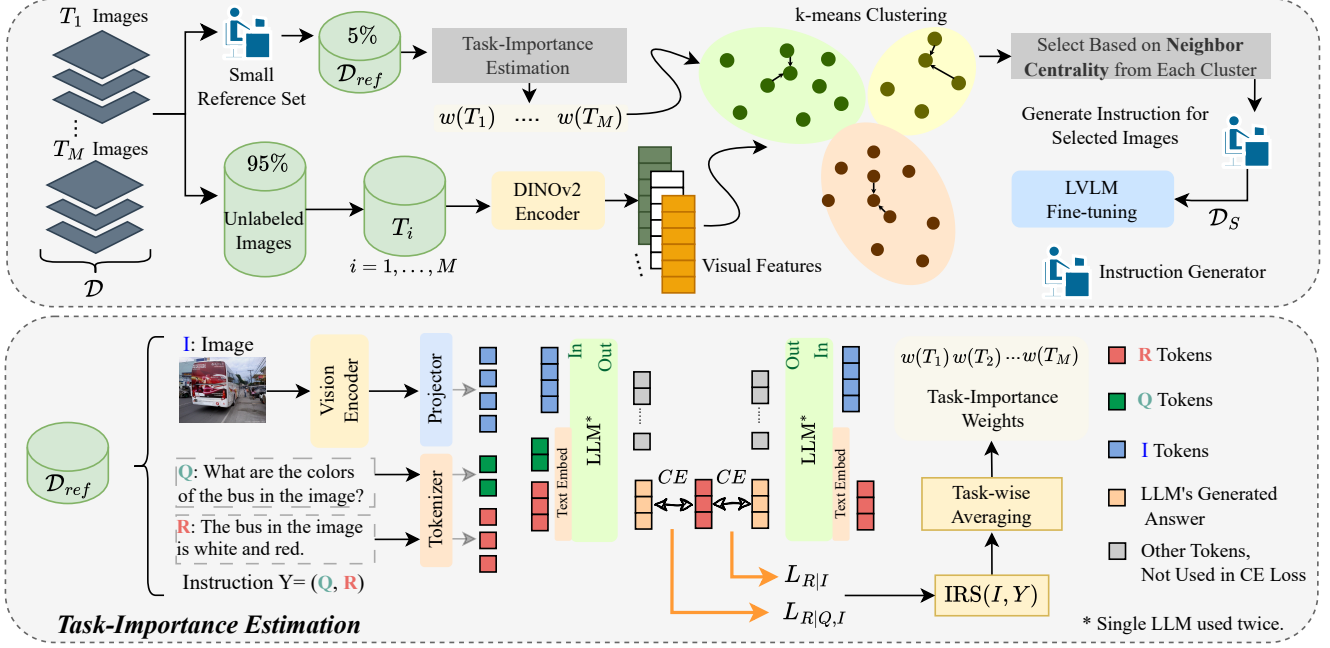


Figure 3. We propose **PreSel**, an efficient **Pre-Instruction Data Selection** approach for Visual Instruction Tuning (VIT). Given a large pool of unlabeled images D from various tasks, **PreSel** first estimates the importance of each task T_i via a randomly selected small reference set D_{ref} with instructions generated. Each instruction (Y) is split into questions (Q) and responses (R) to compute the Instruction Relevance Score (IRS), which determines task proportions $w(T_i)$ in the final selected subset D_S . Given the derived task proportions, it then uses the DINOv2 vision encoder to extract features from the remaining unlabeled images, perform clustering within each task, and select representative images using the Neighbor Centrality (NC) score. The collection of selected images from all tasks is assembled as D_S .

evaluates how much the provided Q contributes to generating the ground-truth response R . Formally, the next-token cross-entropy (CE) loss for R given the tokens of I and Q as context is as follows:

$$\mathcal{L}_{R|Q,I} = -\frac{1}{|\mathbf{t}^R|} \sum_{j=1}^{|\mathbf{t}^R|} \log P_\theta(t_j^R | I, Q, \mathbf{t}_{<j}^R), \quad (1)$$

where \mathbf{t}^R is the tokenized R with $|\mathbf{t}^R|$ tokens, and $\mathbf{t}_{<j}^R$ is the sequence of tokens preceding the j -th token in R . P_θ denotes the predicted probability distribution of the reference model, parameterized by θ . We then calculate the loss without the Q given as context:

$$\mathcal{L}_{R|I} = -\frac{1}{|\mathbf{t}^R|} \sum_{j=1}^{|\mathbf{t}^R|} \log P_\theta(t_j^R | I, \mathbf{t}_{<j}^R), \quad (2)$$

where the response is only conditioned on the image context. The proposed IRS is formulated as the ratio of these two losses as follows:

$$\text{IRS} = \frac{\mathcal{L}_{R|Q,I}}{\mathcal{L}_{R|I}}. \quad (3)$$

A higher IRS indicates that adding the Q context to I does not assist in refining the model for easier generation of R . In contrast, a lower IRS shows that the model's confusion regarding R is reduced when Q is provided as input,

emphasizing the necessity of Q for VIT. We then compute the average IRS over all samples in D_{ref} that belong to task T_i as follows:

$$s(T_i) = \frac{1}{|D_{ref}^i|} \sum_{I \in T_i} \text{IRS}(I, Y), \quad (4)$$

where $|D_{ref}^i|$ denotes the number of samples in D_{ref} that belong to T_i . Based on the definition of IRS, a lower $s(T_i)$ indicates a higher importance of T_i . The final relative proportion of each task within D_S is defined as:

$$w(T_i) = \frac{\exp(-s(T_i)/\tau)}{\sum_{j=1}^M \exp(-s(T_j)/\tau)}, \quad (5)$$

where we set the temperature value $\tau = \frac{1}{\sqrt{M}}$.

3.2. Task-wise Cluster-based Selection

After determining the relative proportion of each task using the reference set, we focus on selecting informative unlabeled images within each task for instruction generation. For the unlabeled images in task T_i , we first extract their visual features using the pre-trained DINOv2 [30] model, a lightweight vision encoder. Specifically, given an input image $I \in T_i$, we obtain the feature vector \mathbf{v}_I from the last transformer layer's [CLS] token after its Layer Normalization. We then cluster these obtained \mathbf{v}_I features of task T_i

into C clusters $\{A_c^i\}_{c=1}^C$ using the k-means [26] algorithm, where we set $C = \frac{|T_i|}{100}$. To select samples from the c -th cluster A_c^i within T_i , we consider both its relative size $|A_c^i|$ and the importance weight $w(T_i)$ of task T_i . Specifically, we choose:

$$n_c = \left\lfloor \frac{w(T_i) \cdot |A_c^i|}{|T_i|} \cdot |\mathcal{D}_S| \right\rfloor \quad (6)$$

images from cluster A_c^i . This approach ensures a diverse selection of images within each cluster, taking into account its size and the overall importance of the corresponding task.

Intra-Cluster Selection. Within each cluster, we select the n_c most representative images based on the *Neighbor Centrality* (*NC*) score, defined as:

$$s_{nc}(I) = \frac{1}{k} \cdot \sum_{I_a \in k\text{NN}(I)} \text{sim}(\mathbf{v}_I, \mathbf{v}_{I_a}). \quad (7)$$

Here we denote the k -nearest neighbors of a given image I in feature space as $k\text{NN}(I)$, and $\text{sim}(\cdot, \cdot)$ is the cosine similarity. A higher s_{nc} indicates that the image is closely situated to its neighbors, implying it is more likely to be a representative sample rather than an outlier.

Finally, the collection of selected images from all tasks is assembled as \mathcal{D}_S . We utilize resources to generate instructions only for images in \mathcal{D}_S , which are then used to fine-tune the LVLM. Figure 3 provides an overview.

4. Experiments

4.1. Experimental Setup

Datasets. We conduct experiments on two large-scale VIT datasets: LLaVA-1.5 [22] and Vision-Flan [44]. LLaVA-1.5, a widely used dataset, comprises more than 600K samples across about 10 different tasks. Vision-Flan includes 191 distinct tasks and 186K data points. Evaluating on this dataset allows us to assess performance when dealing with a high number of tasks and relatively fewer images per task. It is important to note that although our approach can be used to efficiently construct new VIT datasets or scale up existing ones, we use these established VIT datasets for evaluation purposes. Specifically, we perform data selection on the unlabeled images and treat the corresponding instructions for the selected images as the generated instructions.

Baselines. We compare our proposed approach with several data selection methods, namely Random, CLIP-Score [33], TypiClust [11], EL2N [31], Perplexity [28], IFD [19], Self-Filter [5], and COINCIDE [15]. In particular, Self-Filter and COINCIDE are recent state-of-the-art VIT data selection methods that are closest to our setting. IFD, EL2N, and Perplexity are state-of-the-art selection methods used for instruction tuning in the NLP domain. Due to the similarity

of our paradigm to active learning (AL) [17, 34, 35, 42], we also transplant and adapt TypiClust, a strong clustering-based AL method, as it cannot be directly applied in our setting. See Section A4 in Appendix for more details of these methods.

Evaluation Benchmarks. We evaluate the performance of different fine-tuned LVLMs across several multimodal evaluation benchmarks, including VQAv2 [10], ScienceQA [25], TextVQA [38], MME-Perception [45], MMBench [23], MM-Bench (Chinese version) [23], SEED-Bench [16], MM-Vet [47], and POPE [20]. This diverse set of metrics effectively assesses the quality of LVLMs fine-tuned with samples selected by the compared methods, covering aspects such as object hallucination, open-ended short answers, scientific question answering, text-intensive VQA, robust yes/no and multiple-choice QA, and visual conversations.

Implementation details. Unless stated otherwise, we set the sampling ratio to 15% of the VIT dataset in all our comparisons and fine-tune the LLaVA-1.5-7B [22] pre-training checkpoint ² (the model before LLaVA’s VIT stage) with the selected VIT samples. The proposed method requires a small, randomly selected reference set \mathcal{D}_{ref} for task-importance estimation, which is equal to 5% of the VIT dataset. At a 15% sampling ratio, we select an additional 10% of data using our method and combine it with the 5% reference set \mathcal{D}_{ref} to ensure fair comparisons. As the scale of different evaluation benchmarks varies, we report the *Average Relative Performance (Rel. %)* in our comparisons. The relative performance for each benchmark is calculated as

$$\frac{\text{The model's performance}}{\text{The full fine-tuned model's performance}} \times 100.$$

In all experiments, we fine-tune the LVLM for one epoch using LoRA [12]. We use the same training details as the official LLaVA-1.5 paper [22]. We conduct all experiments using four H100 (80 GB) GPUs.

4.2. Main Results

High performance with minimal instruction generation. Table 1 presents the results on the LLaVA-1.5 dataset, comparing PreSel with various data selection baselines to highlight its efficiency. We set the sampling ratio to 15% of the full LLaVA-1.5 size. It can be observed that the proposed method significantly outperforms other baselines in average relative performance and achieves comparable performance to full-scale LLaVA fine-tuning. Notably, this performance gain is achieved with instruction generation for only the selected 15% of images, as shown in the *Required Instructions* column. Interestingly, random selection outperforms

²This checkpoint is taken after pre-training the projector for feature alignment but before the VIT stage.: <https://huggingface.co/liushaotian/llava-v1.5-mlp2x-336px-pretrain-vicuna-7b-v1.5>.

Method	Req. Inst.	Sel. Inst.	VQAv2	SQA-I	TextVQA	MME	MMBench		SEED-Bench	MM-Vet	POPE	Rel. (%)
							en	cn				
BLIP-2 [ICML-23] [18]	100%	-	65.0	61.0	42.5	1293.8	-	-	49.7	22.4	85.3	-
InstructBLIP-7B [NeurIPS-23] [7]	100%	1.2M	-	60.5	50.1	-	36.0	23.7	58.8	26.2	-	-
Shikra [Arxiv-23] [4]	100%	5.5M	77.4	-	-	-	58.8	-	-	-	-	-
IDEFICS-80B [HuggingFace-23] [14]	100%	1M	60.0	-	30.9	-	54.5	38.1	53.2	-	-	-
Qwen-VL-Chat [Arxiv-23] [2]	100%	50M	78.2	68.2	61.5	1487.5	60.6	56.7	65.4	-	-	-
InstructionGPT-4 [Arxiv-23] [40]	100%	0.2K	-	-	20.6	463.3	31.4	-	-	-	-	-
LLaVA-1.5-7B	100%	665K	79.1	68.4	57.9	1417.6	66.0	58.9	66.8	30.0	87.5	100
Random	15%	93K	75.3	67.8	54.3	1397.5	61.0	53.5	62.4	<u>30.2</u>	84.9	95.7
TypiClust [ICML-22] [11]	15%	93K	<u>76.0</u>	<u>68.2</u>	53.3	1396.2	<u>64.3</u>	57.1	<u>62.8</u>	29.7	85.6	<u>96.8</u>
CLIP-Score [ICML-21] [33]	100%	93K	71.7	64.5	53.4	1380.3	51.0	48.0	56.2	29.9	84.0	90.3
EL2N [NeurIPS-21] [31]	100%	93K	76.1	66.5	50.2	1405.2	58.2	48.5	61.8	30.0	83.3	93.0
Perplexity [Arxiv-23] [28]	100%	93K	73.1	67.2	54.6	1283.7	54.7	47.8	58.3	30.7	85.5	91.9
IFD [NAACL-24] [19]	100%	93K	74.0	66.5	51.8	1307.2	57.2	50.6	59.4	28.1	<u>86.6</u>	91.8
Self-Filter [ACL-24] [5]	100%	93K	74.0	62.3	51.4	1356.5	48.1	45.4	56.3	29.0	87.0	88.8
COINCIDE [EMNLP-24] [15]	100%	93K	76.1	67.7	<u>54.8</u>	1414.9	60.5	53.9	62.0	28.5	86.4	95.5
PreSel (Ours)	15%	93K	75.0	70.1	55.2	1457.7	64.8	<u>56.5</u>	63.8	29.6	85.4	97.9

Table 1. **Results on the LLaVA-1.5 dataset.** We compare **PreSel** with several data selection approaches across multiple multimodal benchmarks. “Sel. Inst.” indicates the number of visual instructions used to fine-tune the LVLM. Our experiments involve selecting 15% of the full VIT dataset (93K samples) for fine-tuning. “Req. Inst.” shows percentage of images for which instructions are generated. **PreSel** only requires instruction generation for the selected images (15%), whereas other methods need instructions for 100% of the data to perform selection. The best result is **bolded** and the runner-up is underlined.

many baselines, even though these methods have access to all instructions prior to selection. This may be because these methods often select a poor distribution of samples across tasks, negatively impacting performance. Also, these methods tend to overly prioritize sample difficulty for generation, neglecting the visual diversity of the selected samples. Our explicit task-importance estimation coupled with representative sample selection from diverse clusters yields a clear performance boost over other baselines. In particular, **PreSel** outperforms Random by 2.2% and the second-best performing baseline by 1.1%, showing its effectiveness.

PreSel is robust across varying task diversities. As the LLaVA-1.5 dataset contains a relatively limited number of tasks (approximately 10), we also conduct experiments on Vision-Flan, which covers a diverse set of 191 vision tasks, as shown in Table 2. The results demonstrate that **PreSel** even slightly surpasses the performance of the full-scale fine-tuned LLaVA model with only 15% generated instructions. This verifies that the proposed approach can robustly adapt to VIT datasets with varying numbers of vision tasks without performance degradation. Particularly, our results on Vision-Flan highlight significant efficiency advantages for creating VIT datasets with a diverse set of tasks, because (1) the task-importance estimation step can automatically identify the important tasks to focus on, and (2) our approach performs selection directly on unlabeled images, generating instructions only for the selected ones. This reduced instruction generation cost enables a more efficient expansion of VIT datasets.

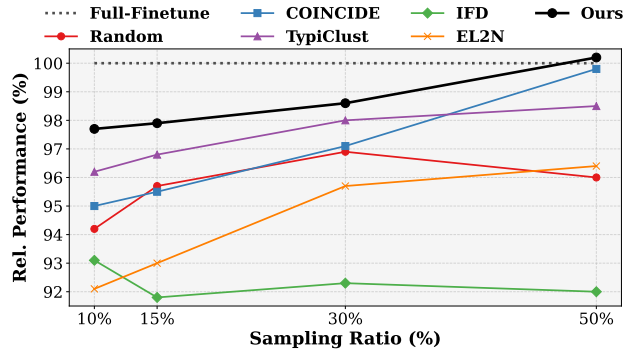


Figure 4. Average relative performance of data selection methods on LLaVA-1.5 at different sampling ratios.

4.3. Detailed Analyses

Performance across various sampling ratios. Figure 4 shows the average relative performance of different approaches on LLaVA-1.5 for sampling ratios from 10% to 50% of the full dataset. Interestingly, the performance of random selection begins to degrade beyond a certain ratio, underscoring that merely adding more data does not always lead to improved VIT performance. Hence, effective data selection is crucial for identifying and incorporating only the most beneficial samples. It can be seen that most data selection methods show performance gains with larger sampling budgets; however, IFD fails to improve. We discovered this occurs because IFD predominantly selects samples from the LLaVA-v1 [21] subset of the LLaVA-1.5 dataset (tasks: LLaVA-Conv,-Detail,-Reason), which comprise al-

Method	Req. Inst.	Sel. Inst.	VQAv2	SQA-I	TextVQA	MME	MMBench		SEED-Bench	MM-Vet	POPE	Rel. (%)
							en	cn				
LLaVA-1.5-7B	100%	186K	69.6	55.6	38.3	1238.1	53.4	48.2	55.6	27.7	85.7	100
Random	15%	28K	66.5	62.1	38.7	1238.6	43.6	43.1	48.3	28.1	83.0	96.1
TypiClust [ICML-22] [11]	15%	28K	65.8	59.2	37.7	1194.1	32.4	45.1	44.9	28.2	81.6	92.0
CLIP-Score [ICML-21] [33]	100%	28K	63.0	62.3	39.7	1058.0	37.5	44.2	44.3	28.0	82.0	92.2
EL2N [NeurIPS-23] [31]	100%	28K	63.6	62.7	<u>42.4</u>	<u>1253.8</u>	44.7	37.7	49.2	27.1	79.5	95.2
Perplexity [Arxiv-23] [28]	100%	28K	<u>66.1</u>	53.3	39.5	1195.0	25.7	39.8	38.8	29.3	83.5	88.2
IFD [NAACL-24] [19]	100%	28K	65.0	57.8	42.0	1210.9	30.4	40.8	39.1	26.9	82.6	90.0
Self-Filter [ACL-24] [5]	100%	28K	64.9	59.3	42.6	1262.2	42.1	43.8	44.5	25.1	80.9	94.2
COINCIDE [EMNLP-24] [15]	100%	28K	66.0	<u>63.9</u>	33.0	1184.4	<u>49.6</u>	<u>48.2</u>	53.9	26.1	84.3	<u>97.1</u>
PreSel (Ours)	15%	28K	64.1	66.2	39.7	1218.8	50.4	<u>45.4</u>	<u>53.5</u>	<u>29.1</u>	<u>84.1</u>	100.1

Table 2. **Results on the Vision-Flan dataset.** We compare PreSel with several data selection approaches across multiple multimodal benchmarks. “Sel. Inst.” indicates the number of visual instructions used to fine-tune the LVLM. Our experiments involve selecting 15% of the full VIT dataset (28K samples) for fine-tuning. “Req. Inst.” shows the percentage of images for which instructions are generated. PreSel only requires instruction generation for the selected images (15%), whereas other methods need instructions for 100% of the data to perform the selection. The best result is **bolded**, and the runner-up is underlined.

Methods	Selection Cost	Finetuning Cost	Inst. Gen. Cost	Total Cost	Rel. (%)
Full Finetune	–	76.0 GPU-hr	$100\% \cdot C$	76.0 GPU-hr + $100\% \cdot C$	100
Self-Filter [5]	73.5 GPU-hr	11.0 GPU-hr	$100\% \cdot C$	84.5 GPU-hr + $100\% \cdot C$	88.8
COINCIDE [15]	55.5 GPU-hr	11.0 GPU-hr	$100\% \cdot C$	66.5 GPU-hr + $100\% \cdot C$	95.5
PreSel (Ours)	9.0 GPU-hr	11.0 GPU-hr	$15\% \cdot C$	20.0 GPU-hr + 15% · C	97.9

Table 3. Comparison of VIT costs for PreSel, other VIT data selection methods, and full-scale LVLM fine-tuning. GPU-hr refers to one H100 (80 GB) GPU used for one hour, and C is the total cost for instruction generation across all unlabeled VIT images.

most 25% of the entire dataset. Both our experiments and prior research [44] indicate that only a few samples from these tasks are needed for strong performance. Consequently, IFD inefficiently allocates its budget to LLaVA-v1, missing more informative samples from other critical tasks. Our task-importance estimation approach effectively tackles this challenge (see Figure 5). Overall, PreSel surpasses the full-finetuning baseline at 50% sampling ratio and consistently delivers superior performance across all ratios.

Cost analysis. Table 3 compares the computational cost of PreSel with two recent VIT data selection methods and full-scale fine-tuning. Using a 15% sampling ratio on the LLaVA-1.5 dataset, PreSel achieves Pareto efficiency improvements in data selection. It selects 15% of images in just 9 GPU hours, whereas COINCIDE and Self-Filter require 55.5 and 73.5 GPU hours, respectively, for 15% of image-instruction pairs. COINCIDE’s high cost stems from TinyLLaVA-2B forward passes on all image-instruction pairs, while PreSel requires DINOv2 forward passes only for images without instructions and LLaVA-1.5-7B forward passes for just 5% of image-instruction pairs (two per sample for IRS computation). The computational cost of PreSel scales linearly with dataset size, ensuring scalability. Self-Filter is inefficient as it requires training an LVLM on all image-instruction pairs before selection.

Additionally, PreSel significantly reduces instruction

generation costs by selecting data directly from unlabeled images, whereas COINCIDE and Self-Filter require generating instructions for all images. In the table, instruction generation costs are denoted as C , a highly expensive process. Overall, PreSel achieves substantial efficiency gains in both GPU usage and instruction generation while maintaining competitive performance with full-scale fine-tuning.

The effect of our Task-Importance Estimation. In Table 4, we present experiments on the LLaVA-1.5 dataset with sampling ratio set to 15% to evaluate the effectiveness of the proposed *Task-Importance Estimation* component within our framework. Specifically, we conduct two sets of experiments. In the top three rows of the table, we use the intra-cluster selection approach *Neighbor Centrality (NC)*, which is the default in PreSel. To completely decouple the effect of our NC component on task-importance estimation, we use Random for intra-cluster selection in the bottom three rows. *Uniform* indicates that we select the same number of images from each task in the VIT dataset, regardless of the size or importance of a particular task; that is, each task will have an equal number of selected samples in \mathcal{D}_S . *Size-Balanced* denotes that the budget for each task is set proportional to its relative size compared to other tasks in the VIT dataset, so larger tasks will have more samples selected in \mathcal{D}_S . *Task-Importance* refers to our proposed approach, where the budget for each task is allocated based on

NC	Balancing	Rel. (%)
✓	Uniform	95.8
	Size-Balanced	97.1
	Task-Importance	97.9
-	Uniform	94.8
	Size-Balanced	94.9
	Task-Importance	96.9

Table 4. The effect of different task balancing strategies on the performance for the LLaVA-1.5 dataset. Ours is Task-Importance.

its estimated importance, as described in Section 3.1. The results in Table 4 confirm the effectiveness of our proposed Task-Importance Estimation approach. Specifically, sampling based on Task-Importance outperforms Size-Balanced sampling by significant margins of 0.8% and 2.0%, with and without the NC component, respectively. Furthermore, we observe that Size-Balanced sampling performs better than Uniform. This is expected, as the size of each task in the LLaVA-1.5 dataset was heuristically adjusted to achieve reasonably good performance during the creation of this VIT dataset [22]. Consequently, Size-Balanced sampling is not entirely arbitrary or random. However, in practice, it is highly expensive to heuristically determine such a size balance across a large number of vision tasks when creating a VIT dataset for a custom application. Our task-importance estimation mechanism effectively automates this step.

In Figure 5, we compare the task proportions assigned by our method to those assigned by Size-Balanced on the LLaVA-1.5 dataset. We observe that Size-Balanced assigns almost 25% of the total budget to the LLaVA-v1 [21] tasks (LLaVA-Conv, -Detail, -Reason). However, our experiments and previous research [15, 44] have shown that a small fraction of these tasks is sufficient for good VIT performance. In contrast, PreSel automatically reduces the allocation to these tasks and assigns more budget to tasks such as A-OKVQA and GQA, which are more integral for VIT [8, 15].

The effect of Neighbor Centrality (NC) and clustering. In Table 5, we conduct ablation studies on LLaVA-1.5 with the sampling ratio set to 15% to verify the effectiveness of the proposed k-means clustering within each task and intra-cluster selection based on NC scores. In the first row, we perform random selection on the images within each task based on the budget, without involving any clustering. In the second row, we apply clustering to each task’s images and randomly sample from each cluster according to the budget defined in Equation 6. The third row is similar to the first, but we select images from each task based on the NC score. Finally, the last row represents the full version of PreSel, which includes both the clustering and NC components. The results confirm the positive contribution of each component to the overall performance, with the complete PreSel achieving the best results.

NC	Clustering	Rel. (%)
-	-	96.2
	✓	96.9
	✓	97.2
✓	-	97.9

Table 5. Ablation study on NC and k-means clustering. The experiments are conducted on the LLaVA-1.5 dataset with the sampling ratio set to 15%.

# of Nearest Neighbors (k)	Rel. (%)
5	97.9
10	98.2
20	97.4
Second-best	96.8

Table 6. Sensitivity to k . The experiments are conducted on LLaVA-1.5 with the sampling ratio set to 15%.

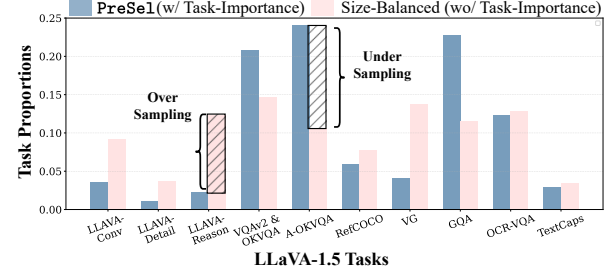


Figure 5. A demonstration of task proportions for the LLaVA-1.5 dataset assigned by PreSel and Size-Balanced sampling.

Sensitivity to the number of nearest neighbors (k). In our NC score calculations, we use a hyperparameter k , which represents the number of nearest samples in feature space considered for computing the NC score. In Table 6, we repeat the experiment on LLaVA-1.5 with the sampling ratio set to 15% for $k = 5, 10, 20$ and evaluate the performance change. We observe that PreSel is quite robust to variations in the value of k , consistently achieving higher average relative performance than the second-best method across all values of k . We set k to 5 in all our experiments.

5. Conclusion

In this paper, we introduce a new data selection paradigm, termed pre-instruction data selection for VIT, which aims to reduce both VIT runtime and instruction generation costs. We propose PreSel, an effective pre-instruction data selection approach that operates directly on unlabeled images before instruction generation. PreSel leverages a novel Task-Importance Estimation mechanism to automatically identify the most impactful vision tasks for budget allocation. It then selects the most beneficial images from each task for instruction annotation, according to the budgets. Our extensive experiments on the LLaVA-1.5 and Vision-Flan datasets demonstrate that PreSel significantly outperforms other state-of-the-art data selection baselines and achieves performance comparable to full-scale fine-tuning of LMs, while requiring instructions for only the selected 15% unlabeled images. PreSel also enables easier creation of multi-task VIT datasets for custom applications under constrained resources.

References

[1] Josh Achiam, Steven Adler, Sandhini Agarwal, Lama Ahmad, Ilge Akkaya, Florencia Leoni Aleman, Diogo Almeida, Janko Altenschmidt, Sam Altman, Shyamal Anadkat, et al. Gpt-4 technical report. *arXiv preprint arXiv:2303.08774*, 2023. 1, 2, 3

[2] Jinze Bai, Shuai Bai, Shusheng Yang, Shijie Wang, Sinan Tan, Peng Wang, Junyang Lin, Chang Zhou, and Jingren Zhou. Qwen-vl: A frontier large vision-language model with versatile abilities. *arXiv preprint arXiv:2308.12966*, 2023. 1, 2, 6

[3] Tom Brown, Benjamin Mann, Nick Ryder, Melanie Subbiah, Jared D Kaplan, Prafulla Dhariwal, Arvind Neelakantan, Pranav Shyam, Girish Sastry, Amanda Askell, et al. Language models are few-shot learners. In *Conference on Neural Information Processing Systems*, 2020. 1, 2, 3

[4] Keqin Chen, Zhao Zhang, Weili Zeng, Richong Zhang, Feng Zhu, and Rui Zhao. Shikra: Unleashing multimodal llm's referential dialogue magic. *arXiv preprint arXiv:2306.15195*, 2023. 6

[5] Ruibo Chen, Yihan Wu, Lichang Chen, Guodong Liu, Qi He, Tianyi Xiong, Chenxi Liu, Junfeng Guo, and Heng Huang. Your vision-language model itself is a strong filter: Towards high-quality instruction tuning with data selection. In *Findings of the Association for Computational Linguistics*, 2024. 2, 3, 5, 6, 7, 12

[6] Wei-Lin Chiang, Zhuohan Li, Zi Lin, Ying Sheng, Zhanghao Wu, Hao Zhang, Lianmin Zheng, Siyuan Zhuang, Yonghao Zhuang, Joseph E. Gonzalez, Ion Stoica, and Eric P. Xing. Vicuna: An open-source chatbot impressing gpt-4 with 90%* chatgpt quality, 2023. <https://lmsys.org/blog/2023-03-30-vicuna>. 2, 11, 12

[7] Wenliang Dai, Junnan Li, Dongxu Li, Anthony Tiong, Junqi Zhao, Weisheng Wang, Boyang Li, Pascale Fung, and Steven Hoi. Instructblip: Towards general-purpose vision-language models with instruction tuning. In *Conference on Neural Information Processing Systems*, 2023. 1, 2, 6

[8] Yanqi Dai, Dong Jing, Nanyi Fei, and Zhiwu Lu. Cotbal: Comprehensive task balancing for multi-task visual instruction tuning. *arXiv preprint arXiv:2403.04343*, 2024. 2, 3, 8

[9] Abhimanyu Dubey, Abhinav Jauhri, Abhinav Pandey, Abhishek Kadian, Ahmad Al-Dahle, Aiesha Letman, Akhil Mathur, Alan Schelten, Amy Yang, Angela Fan, et al. The llama 3 herd of models. *arXiv preprint arXiv:2407.21783*, 2024. 2, 11, 12

[10] Yash Goyal, Tejas Khot, Douglas Summers-Stay, Dhruv Batra, and Devi Parikh. Making the v in vqa matter: Elevating the role of image understanding in visual question answering. In *IEEE/CVF Conference on Computer Vision and Pattern Recognition*, 2017. 1, 5

[11] Guy Hacohen, Avihu Dekel, and Daphna Weinshall. Active learning on a budget: Opposite strategies suit high and low budgets. In *International Conference on Machine Learning*, 2022. 5, 6, 7, 11

[12] Edward J Hu, Yelong Shen, Phillip Wallis, Zeyuan Allen-Zhu, Yuanzhi Li, Shean Wang, Lu Wang, and Weizhu Chen. Lora: Low-rank adaptation of large language models. *arXiv preprint arXiv:2106.09685*, 2021. 5

[13] Sahar Kazemzadeh, Vicente Ordonez, Mark Matten, and Tamara Berg. Referitgame: Referring to objects in photographs of natural scenes. In *Conference on Empirical Methods in Natural Language Processing*, 2014. 1

[14] Hugo Laurencon, Daniel van Strien, Stas Bekman, Leo Tronchon, Lucile Saulnier, Thomas Wang, Siddharth Karamcheti, Amanpreet Singh, Giada Pistilli, Yacine Jernite, and Victor Sanh. Introducing idefics: An open reproduction of state-of-the-art visual language model, 2023. <https://huggingface.co/blog/idefics>. 6

[15] Jaewoo Lee, Boyang Li, and Sung Ju Hwang. Concept-skill transferability-based data selection for large vision-language models. In *Conference on Empirical Methods in Natural Language Processing*, 2024. 2, 3, 5, 6, 7, 8, 12

[16] Bohao Li, Rui Wang, Guangzhi Wang, Yuying Ge, Yixiao Ge, and Ying Shan. Seed-bench: Benchmarking multimodal llms with generative comprehension. *arXiv preprint arXiv:2307.16125*, 2023. 5

[17] Dongyuan Li, Zhen Wang, Yankai Chen, Renhe Jiang, Weiping Ding, and Manabu Okumura. A survey on deep active learning: Recent advances and new frontiers. *IEEE Transactions on Neural Networks and Learning Systems*, 2024. 5

[18] Junnan Li, Dongxu Li, Silvio Savarese, and Steven Hoi. Blip-2: Bootstrapping language-image pre-training with frozen image encoders and large language models. In *International Conference on Machine Learning*, 2023. 6

[19] Ming Li, Yong Zhang, Zhitao Li, Juhai Chen, Lichang Chen, Ning Cheng, Jianzong Wang, Tianyi Zhou, and Jing Xiao. From quantity to quality: Boosting llm performance with self-guided data selection for instruction tuning. In *Conference of the Nations of the Americas Chapter of the Association for Computational Linguistics*, 2024. 2, 3, 5, 6, 7, 12

[20] Yifan Li, Yifan Du, Kun Zhou, Jinpeng Wang, Wayne Xin Zhao, and Ji-Rong Wen. Evaluating object hallucination in large vision-language models. *arXiv preprint arXiv:2305.10355*, 2023. 5

[21] Haotian Liu, Chunyuan Li, Qingyang Wu, and Yong Jae Lee. Visual instruction tuning. In *Conference on Neural Information Processing Systems*, 2023. 1, 2, 6, 8

[22] Haotian Liu, Chunyuan Li, Yuheng Li, and Yong Jae Lee. Improved baselines with visual instruction tuning. In *IEEE/CVF Conference on Computer Vision and Pattern Recognition*, 2024. 1, 2, 5, 8

[23] Yuan Liu, Haodong Duan, Yuanhan Zhang, Bo Li, Songyang Zhang, Wangbo Zhao, Yike Yuan, Jiaqi Wang, Conghui He, Ziwei Liu, et al. Mmbench: Is your multi-modal model an all-around player? In *European Conference on Computer Vision*, 2024. 5

[24] Zikang Liu, Kun Zhou, Wayne Xin Zhao, Dawei Gao, Yaliang Li, and Ji-Rong Wen. Less is more: Data value estimation for visual instruction tuning. *arXiv preprint arXiv:2403.09559*, 2024. 2, 3

[25] Pan Lu, Swaroop Mishra, Tanglin Xia, Liang Qiu, Kai-Wei Chang, Song-Chun Zhu, Oyvind Tafjord, Peter Clark, and

Ashwin Kalyan. Learn to explain: Multimodal reasoning via thought chains for science question answering. *Conference on Neural Information Processing Systems*, 2022. 5

[26] J MacQueen. Some methods for classification and analysis of multivariate observations. In *Berkeley Symposium on Mathematical Statistics and Probability*, 1967. 5

[27] Kenneth Marino, Mohammad Rastegari, Ali Farhadi, and Roozbeh Mottaghi. Ok-vqa: A visual question answering benchmark requiring external knowledge. In *IEEE/CVF Conference on Computer Vision and Pattern Recognition*, 2019. 1

[28] Max Marion, Ahmet Üstün, Luiza Pozzobon, Alex Wang, Marzieh Fadaee, and Sara Hooker. When less is more: Investigating data pruning for pretraining llms at scale. *arXiv preprint arXiv:2309.04564*, 2023. 3, 5, 6, 7, 11

[29] Anand Mishra, Shashank Shekhar, Ajeet Kumar Singh, and Anirban Chakraborty. Ocr-vqa: Visual question answering by reading text in images. In *International Conference on Document Analysis and Recognition*, 2019. 1

[30] Maxime Oquab, Timothée Darcret, Théo Moutakanni, Huy Vo, Marc Szafraniec, Vasil Khalidov, Pierre Fernandez, Daniel Haziza, Francisco Massa, Alaaeldin El-Nouby, et al. Divenov2: Learning robust visual features without supervision. In *Transactions on Machine Learning Research*, 2024. 2, 3, 4

[31] Mansheej Paul, Surya Ganguli, and Gintare Karolina Dziugaite. Deep learning on a data diet: Finding important examples early in training. In *Conference on Neural Information Processing systems*, 2021. 5, 6, 7, 11

[32] Baolin Peng, Chunyuan Li, Pengcheng He, Michel Galley, and Jianfeng Gao. Instruction tuning with gpt-4. *arXiv preprint arXiv:2304.03277*, 2023. 1, 2

[33] Alec Radford, Jong Wook Kim, Chris Hallacy, Aditya Ramesh, Gabriel Goh, Sandhini Agarwal, Girish Sastry, Amanda Askell, Pamela Mishkin, Jack Clark, et al. Learning transferable visual models from natural language supervision. In *International Conference on Machine Learning*, 2021. 2, 5, 6, 7, 11

[34] Bardia Safaei and Vishal M. Patel. Active learning for vision language models. In *Proceedings of the Winter Conference on Applications of Computer Vision (WACV)*, pages 4902–4912, 2025. 5

[35] Bardia Safaei, VS Vibashan, Celso M de Melo, and Vishal M Patel. Entropic open-set active learning. In *Proceedings of the AAAI conference on artificial intelligence*, pages 4686–4694, 2024. 5

[36] Dustin Schwenk, Apoorv Khandelwal, Christopher Clark, Kenneth Marino, and Roozbeh Mottaghi. A-okvqa: A benchmark for visual question answering using world knowledge. In *European Conference on Computer Vision*, 2022. 1

[37] Oleksii Sidorov, Ronghang Hu, Marcus Rohrbach, and Amanpreet Singh. Textcaps: a dataset for image captioning with reading comprehension. In *European Conference on Computer Vision*, 2020. 1

[38] Amanpreet Singh, Vivek Natarajan, Meet Shah, Yu Jiang, Xinlei Chen, Dhruv Batra, Devi Parikh, and Marcus Rohrbach. Towards vqa models that can read. In *IEEE/CVF Conference on Computer Vision and Pattern Recognition*, 2019. 5

[39] Shengbang Tong, Ellis Brown, Penghao Wu, Sanghyun Woo, Manoj Middepogu, Sai Charitha Akula, Jihan Yang, Shusheng Yang, Adithya Iyer, Xichen Pan, Austin Wang, Rob Fergus, Yann LeCun, and Saining Xie. Cambrian-1: A fully open, vision-centric exploration of multimodal llms. In *Conference on Neural Information Processing Systems*, 2024. 2

[40] Lai Wei, Zihao Jiang, Weiran Huang, and Lichao Sun. Instructiongpt-4: A 200-instruction paradigm for fine-tuning minigpt-4. *arXiv preprint arXiv:2308.12067*, 2023. 2, 6

[41] Mengzhou Xia, Sadhika Malladi, Suchin Gururangan, Sanjeev Arora, and Danqi Chen. Less: Selecting influential data for targeted instruction tuning. In *International Conference on Machine Learning*, 2024. 2

[42] Yichen Xie, Han Lu, Junchi Yan, Xiaokang Yang, Masayoshi Tomizuka, and Wei Zhan. Active finetuning: Exploiting annotation budget in the pretraining-finetuning paradigm. In *Proceedings of the IEEE/CVF Conference on Computer Vision and Pattern Recognition*, pages 23715–23724, 2023. 5

[43] Hu Xu, Saining Xie, Xiaoqing Ellen Tan, Po-Yao Huang, Russell Howes, Vasu Sharma, Shang-Wen Li, Gargi Ghosh, Luke Zettlemoyer, and Christoph Feichtenhofer. Demystifying clip data. In *International Conference on Learning Representations*, 2024. 2

[44] Zhiyang Xu, Chao Feng, Rulin Shao, Trevor Ashby, Ying Shen, Di Jin, Yu Cheng, Qifan Wang, and Lifu Huang. Visionflan: Scaling human-labeled tasks in visual instruction tuning. In *Findings of the Association for Computational Linguistics*, 2024. 1, 2, 5, 7, 8

[45] Shukang Yin, Chaoyou Fu, Sirui Zhao, Ke Li, Xing Sun, Tong Xu, and Enhong Chen. A survey on multimodal large language models. *arXiv preprint arXiv:2306.13549*, 2023. 5

[46] Zhenfei Yin, Jiong Wang, Jianjian Cao, Zhelun Shi, Dingning Liu, Mukai Li, Xiaoshui Huang, Zhiyong Wang, Lu Sheng, Lei Bai, et al. Lamm: Language-assisted multi-modal instruction-tuning dataset, framework, and benchmark. In *Conference on Neural Information Processing Systems*, 2023. 1

[47] Weihao Yu, Zhengyuan Yang, Linjie Li, Jianfeng Wang, Kevin Lin, Zicheng Liu, Xinchao Wang, and Lijuan Wang. Mm-vet: Evaluating large multimodal models for integrated capabilities. *arXiv preprint arXiv:2308.02490*, 2023. 5

[48] Baichuan Zhou, Ying Hu, Xi Weng, Junlong Jia, Jie Luo, Xien Liu, Ji Wu, and Lei Huang. Tinyllava: A framework of small-scale large multimodal models. *arXiv preprint arXiv:2402.14289*, 2024. 12

[49] Chunting Zhou, Pengfei Liu, Puxin Xu, Srinivasan Iyer, Jiao Sun, Yuning Mao, Xuezhe Ma, Avia Efrat, Ping Yu, Lili Yu, et al. Lima: Less is more for alignment. In *Conference on Neural Information Processing Systems*, 2023. 2

[50] Deyao Zhu, Jun Chen, Xiaoqian Shen, Xiang Li, and Mohamed Elhoseiny. Minigpt-4: Enhancing vision-language understanding with advanced large language models. In *International Conference on Learning Representations*, 2024. 1, 2

A1. Limitations and Potential Societal Impacts

Limitations. Currently, our approach utilizes the reference instructions for task-importance estimation. However, given the multimodal nature of LVLMs, these instructions may also be leveraged to improve the selection process on unlabeled images. We leave this limitation as an interesting direction for future work.

Potential Negative Societal Impacts. The proposed method could potentially enable malicious actors to fine-tune open-source LVLMs more easily for illegal purposes. The integration of machine learning security mechanisms could be studied to mitigate such risks.

A2. Different Model Sizes and Architectures

PreSel adapts to various model sizes and architectures. In addition to the results presented in Table 1 and Table 2, which are based on the LLaVA-7B model using Vicuna-7B [6] as the LLM, we conduct two additional sets of experiments on the LLaVA-1.5 dataset, as shown in Table 7. In these experiments, we change the LLM to Vicuna-13B [6] and Llama-8B [9] to evaluate the transferability of the samples selected by PreSel across different model sizes and architectures. It is important to note that we directly use the samples selected by PreSel with LLaVA-7B as the reference model to fine-tune the additional LVLMs, without any further processing. From the table, it is evident that our selected samples are highly beneficial for fine-tuning LVLMs with different architectures or sizes. Specifically, PreSel outperforms Random by large margins of 1.7% and 1.2% in average relative performance for the LLaVA-Vicuna-13B and LLaVA-Llama-8B models, respectively.

A3. More Analysis on the Size of Reference Set

We leverage a small, randomly selected set of image-instruction pairs as the reference set, \mathcal{D}_{ref} , to estimate task-importance values during the Task-Importance Estimation stage. By default, the size of \mathcal{D}_{ref} is set to 5% of the total size of the VIT dataset, \mathcal{D} . In Table 8, we reduce the reference set size to just 1% of the total VIT dataset to evaluate the effect of $|\mathcal{D}_{ref}|$ on the average relative performance. The rest of the experimental settings are identical to those in Table 1 of the main paper: we set the sampling ratio to 15% and conduct experiments on the LLaVA-1.5 dataset. Our experiments show that the estimated task-importance values remain almost identical for both the 1% and 5% cases. Consequently, the final performance is robust to the size of the reference set, as shown in Table 8.

A4. Baselines

In this section, we provide details about the baselines with which we compared our method.

Algorithm 1 Our Proposed PreSel Approach

```

1: Input:
2:   unlabeled images  $\mathcal{D} = \bigcup_{i=1}^M T_i$  where  $T_i$  is the  $i$ -th task, number of vision tasks  $M$ , a lightweight vision encoder (DINOv2), our LVLM, the small randomly selected reference set  $\mathcal{D}_{ref}$ 
3: Process:
4:    $\mathcal{D}_S \leftarrow \emptyset$  # Initialization for the Selected Subset
5:   # Task-Importance Estimation
6:   for each  $(I, Q, R) \in \mathcal{D}_{ref}$ : calculate  $\mathcal{L}_{R|Q,I}$  and  $\mathcal{L}_{R|I}$  via Eq. 1 and Eq. 2 to obtain IRS via Eq. 3
7:   for  $i = 1, \dots, M$  do
8:     calculate  $s(T_i)$  and  $w(T_i)$  via Eq. 4 and Eq. 5
9:   # Task-wise Cluster-based Selection
10:  for  $i = 1, \dots, M$  do
11:     $\mathcal{D}_{T_i} \leftarrow \emptyset$  # Selected Images for Task  $T_i$ 
12:    for unlabeled images in  $T_i$ , extract visual features using DINOv2 encoder as shown in Eq. ???
13:    cluster visual features in  $T_i$  into  $C$  clusters
14:     $\{A_c^i\}_{c=1}^C$  where  $C = \frac{|T_i|}{100}$ 
15:    # Intra-Cluster Selection.
16:    for  $c = 1, \dots, C$  do
17:      for  $A_c^i$ , set the cluster budget  $n_c$  via Eq. 6
18:      calculate  $s_{nc}$  for all images within  $A_c^i$  via Eq. 7
19:      rank images in  $A_c^i$  based on  $s_{nc}$  and select the top  $n_c$  samples with the highest values  $\mathcal{D}_{T_i}^c$ 
20:       $\mathcal{D}_{T_i} \leftarrow \mathcal{D}_{T_i} \cup \mathcal{D}_{T_i}^c$ 
21:    acquire instructions for images in  $\mathcal{D}_{T_i}$ 
22:     $\mathcal{D}_S \leftarrow \mathcal{D}_{T_1} \cup \mathcal{D}_{T_2}, \dots \cup \mathcal{D}_{T_M} \cup \mathcal{D}_{ref}$ 
23:    # Visual Instruction Tuning
24:  fine-tune the LVLM
25:  Return the fine-tuned LVLM

```

- **CLIP-Score [33].** In CLIP-Score, the cosine similarity between the images and their corresponding textual instructions is used for selection. In our experiments, we select samples with high similarity.
- **TypiClust [11].** TypiClust is an active learning approach originally designed for multi-round data selection for image classification under low-budget regimes. It adaptively clusters the unlabeled data and selects the most typical samples from the clusters that have the highest number of unlabeled samples and the fewest already labeled samples. We adapt a single-round version of this method to our setting.
- **EL2N [31].** This method uses the Error L2-Norm (EL2N) to quantify a sample’s informativeness. Specifically, it calculates the average L2-Norm distance between generated tokens and ground-truth text tokens to produce this score.
- **Perplexity [28].** This method uses the average next-token prediction loss as a measure of the LVLM’s uncertainty with respect to a sample. Following prior research [28],

Model	Method	VQAv2	SQA-I	TextVQA	MME	MMBench		SEED-Bench	MM-Vet	POPE	Rel.
		en	cn								
Vicuna-13B [6]	Full Finetune	80.0	72.0	58.3	1400.4	68.2	60.7	68.0	34.3	87.1	100
	Random	76.2	69.9	56.8	1452.3	62.8	56.0	65.0	33.0	86.6	96.6
	PreSel (Ours)	76	70.8	57.0	1404.3	66.4	60.9	65.0	34.4	87.2	98.3
Llama-3-8B [9]	Full Finetune	81.4	78.2	63.8	1561.2	75.2	73.1	71.8	36.9	85.6	100
	Random	77.5	78.3	59.8	1455.0	72.5	69.1	68.3	35.7	84.9	96.0
	PreSel (Ours)	77.0	79.0	59.2	1501.4	73.3	70.6	68.5	37.7	84.6	97.2

Table 7. **Results for LLaVA-Vicuna-13B and LLaVA-Llama-8B models.** We report the performance of **PreSel** across different model architectures and sizes. The experiments are conducted on the LLaVA-1.5 dataset and the sampling ratio is set to 15% for both Random and **PreSel** methods. We directly use the samples acquired for the LLaVA-Vicuna-7B model to fine-tune the additional LVLMs in this experiment. The average relative performance across all evaluation benchmarks is reported.

$\frac{ \mathcal{D}_{\text{ref}} }{ \mathcal{D} }$	Method	VQAv2	SQA-I	TextVQA	MME	MMB-E	MMB-C	SEED-Bench	MM-Vet	POPE	Rel. (%)
-	Full Finetune	79.1	68.4	57.9	1417.6	66.0	58.9	66.8	30.0	87.5	100
	PreSel	75.0	70.1	55.2	1457.7	64.8	56.5	63.8	29.6	85.4	97.9
	PreSel	74.9	69.7	54.2	1436.5	63.1	57.4	63.9	30.0	86.5	97.7

Table 8. The effect of $|\mathcal{D}_{\text{ref}}|$ on average relative performance. The experiments are conducted on the LLaVA-1.5 dataset and the sampling ratio is set to 15%. “Full Finetune” denotes a LLaVA-1.5-7B model fine-tuned on the entire LLaVA-1.5 image-instruction pairs.

we select samples with medium score values instead of top values, as it leads to better results.

- **IFD** [19]. This method proposes the Instruction-Following Difficulty (IFD) metric to select samples with corresponding instructions that have a minimal impact on the model’s loss.
- **Self-Filter** [5]. The Self-Filter method involves initially training a score-net while fine-tuning LVLM on the entire VIT dataset. Afterwards, the score-net is employed to choose a subset of data for a subsequent VIT round. Nonetheless, this two-step procedure escalates the total training expense, opposing the purpose of data selection.
- **COINCIDE** [15]. This method first utilizes the TinyLLaVA-2B [48] model to extract both image and instruction features from multiple layers. It then concatenates all features, performs spherical clustering on them, and selects samples from clusters proportional to their overall transferability.

A5. ShareGPT Data in LLaVA-1.5 Dataset

The LLaVA-1.5 dataset includes a task named ShareGPT, comprised of text-only instructions generated by the ShareGPT model. In our experiments, we have excluded these text-only instructions as our primary focus is to select the most beneficial ‘images’ for visual instruction tuning. One can easily choose a subset of ShareGPT data or use all of it along with our selected VIT samples for fine-tuning LVLMs.

A6. Detailed Algorithm for **PreSel**

We elaborate on the details of our **PreSel** pre-instruction data selection approach in Algorithm 1.